BIOMATERIALS

Control of nacre biomineralization by Pif80 in pearl oyster

So Yeong Bahn,[1] Byung Hoon Jo,[2] Yoo Seong Choi,[3]* Hyung Joon Cha[1]*

Molluscan nacre is a fascinating biomineral consisting of a highly organized calcium carbonate composite that provides unique fracture toughness and an iridescent color. Organisms elaborately control biomineralization using organic macromolecules. We propose the involvement of the matrix protein Pif80 from the pearl oyster *Pinctada fucata* in the development of the inorganic phase during nacre biomineralization, based on experiments using the recombinant form of Pif80. Through interactions with calcium ions, Pif80 participates in the formation of polymer-induced liquid precursor–like amorphous calcium carbonate granules and stabilizes these granules by forming calcium ion–induced coacervates. At the calcification site, the disruption of Pif80 coacervates destabilizes the amorphous mineral precursors, resulting in the growth of a crystalline structure. The redissolved Pif80 controls the growth of aragonite on the polysaccharide substrate, which contributes to the formation of polygonal tablet structure of nacre. Our findings provide insight into the use of organic macromolecules by living organisms in biomineralization.

INTRODUCTION

In nature, many living organisms elaborately control the formation of biominerals for specialized functions, such as mechanical support, protection, and mineral storage. The molluscan shell is one of the most abundant biominerals and protects the internal soft body against predators and mechanical damages. The shell is generally composed of two mineralized layers: the outer (prismatic) layer made of the calcite phase of calcium carbonate ($CaCO_3$) and the inner (nacreous) layer made of the aragonite phase of $CaCO_3$ (*1*). The prismatic layer provides resistance to penetration because of its brittle and hard properties, whereas the nacreous layer, also called nacre, provides resistance to fracture by dissipating energy and exhibits a remarkable iridescent optical property (*1*, *2*). Nacre shows resistance to fracture two or three orders of magnitude higher than that of pure $CaCO_3$, and this mechanical performance is thought to originate from the hierarchical organization of its organic and inorganic components (*1*, *3*, *4*). This fascinating natural composite has been highlighted as a model of biomineralization, and the nacre of mollusks, including bivalves and gastropods, has been widely investigated at the physiological, structural, and molecular levels (*5*–*7*).

Although the mantle epithelial cells are spatially separated from the surface of nacre by the extrapallial space, these cells intimately control the nacre formation by preparing the mineralization components such as inorganic precursors and organic macromolecules and distribute them to the extrapallial space (*7*–*9*). A more detailed strategy for the preparation of biomineralization by the mantle cells has been suggested (*7*, *10*): The mantle cells produce a transient disordered phase of the mineral in intracellular vesicles by concentrating mineral ions and then transporting the mineral precursor to the site of mineral deposition. There, crystallization of nacreous aragonite from the mineral precursor is induced by an organic matrix. It has been proposed and widely accepted that acidic proteins in the organic matrix regulate the stability and polymorphism of $CaCO_3$ at the molecular level (*11*–*13*); several acidic proteins identified in mollusks have been shown to contribute to the stabilization of disordered minerals and/or the mineralization of nacre-like aragonites (*14*–*16*). However, the molecular and biochemical mechanisms involved in the mineralization pathway, including the stabilization and destabilization of the disordered mineral phase and the development of the mineral to the highly organized end product, are not well understood.

Pif80 was discovered in the nacreous layer of the pearl oyster *Pinctada fucata*, a mollusk whose biomineralization process is the basis of much research (*15*). Pif80 is the C-terminal region of the Pif protein. This region, along with the N-terminal Pif97, results from posttranslational proteolytic cleavage (*15*). Pif has drawn much attention because of its indispensability in normal nacre formation, its contribution to the crystallization of nacre-like aragonites (*15*), and the wide distribution of its homologs from bivalves to gastropods (*17*). While the role of Pif97 can be readily inferred by its annotated domain structure (*18*), the specific role of Pif80 has not been determined because of the absence of predictable functional domains. Nevertheless, Pif80 has interesting structural features such as a high ratio of charged and repetitive amino acid residues and the presence of a cluster of acidic amino acid residues. In addition, Pif80 has been suggested to play a crucial role in nacreous aragonite crystallization based on in vivo immunolocalization of Pif80 and its specific binding ability to the aragonite phase of $CaCO_3$ (*15*).

Here, we propose functional roles for Pif80 in both stabilization of the disordered mineral phase and controlled crystallization of aragonite in the nacre formation pathway. Because natural Pif80 forms a protein complex with Pif97 and other matrix proteins (*15*), making isolation of Pif80 and subsequent biochemical characterization extremely difficult, we used recombinant Pif80 (rPif80) synthesized in *Escherichia coli* to investigate the biological roles of Pif80 in nacre formation.

RESULTS

Preparation of rPif80 in a bacterial system

To evaluate the suitability of Pif80 for recombinant expression in a bacterial system, we tested whether native Pif80 has any posttranslational modifications (PTMs). We used periodic acid–Schiff staining and Pro-Q Diamond staining to show that native Pif80 does not exhibit either glycosylation or phosphorylation, the most commonly observed PTMs, although other PTMs may exist (fig. S1, A and B). A similar result was

[1]Department of Chemical Engineering, Pohang University of Science and Technology, Pohang 37673, Korea. [2]Division of Life Science and Research Institute of Life Science, Gyeongsang National University, Jinju 52828, Korea. [3]Department of Chemical Engineering and Applied Chemistry, Chungnam National University, Daejeon 34134, Korea. *Corresponding author. Email: biochoi@cnu.ac.kr (Y.S.C.); hjcha@postech.ac.kr (H.J.C.)

observed for native Pif97 (*18*). Native Pif80 in its denatured state has been shown to be functional in in vitro mineralization (*15*), indicating that the particular conformation of Pif80 is not critical to its proper function. This inference is also supported by the fact that native Pif80 exhibits a high degree of intrinsic disorder (*19*). Thus, the use of a bacterial system seems to be suitable for the recombinant production of Pif80. The coding sequence of the repetitive Pif80 protein was redesigned for genetic stability and efficient expression in *E. coli*. As a result, rPif80 protein was successfully expressed in a soluble form, as confirmed using SDS–polyacrylamide gel electrophoresis (SDS-PAGE) and Western blot analyses (Fig. 1, A and B). The protein was successfully purified using hexahistidine (His_6) tag affinity chromatography followed by size exclusion chromatography with a final yield of 7 mg/liter culture and a purity of approximately 90% according to gel image analysis (Fig. 1C). The unusual acidic property [that is, a calculated isoelectric point (pI) of 5.14] of rPif80 resulted in slower mobility than expected because of negative charge repulsion with SDS in SDS-PAGE (*20*). The molecular mass of rPif80 (55.0 kDa), determined by matrix-assisted laser desorption/ionization–time-of-flight mass spectrometry (MALDI-TOF MS), was nearly identical to the theoretical value (55.4 kDa) (Fig. 1D). Together, these results suggest that rPif80 produced in *E. coli* is expected to be functionally equivalent to the native protein.

Formation of Ca^{2+}-induced rPif80 coacervates

Liquid-liquid phase separation, also known as coacervation, is the spontaneous formation of two immiscible liquid phases from a homogeneous polyelectrolyte solution by the loss of solvation, giving a polyelectrolyte-rich dense (coacervate) phase and a diluted phase (*21*, *22*). We found that the addition of Ca^{2+} to a solution of rPif80 induced a fluidic phase separation, in which stable protein-rich dense fluidic droplets were formed in solutions (pH ~6) containing chlorine or bicarbonate (from supersaturated $CaCO_3$ solution) as counter ions (Fig. 1, E and F). The formation of coacervates was strongly dependent on the concentration of Ca^{2+} (Fig. 1G), whereas pH did not significantly affect the coacervation of rPif80 in the biologically relevant pH range of 7 to 9 (moderately basic condition) found in tissues and the extrapallial fluid of marine

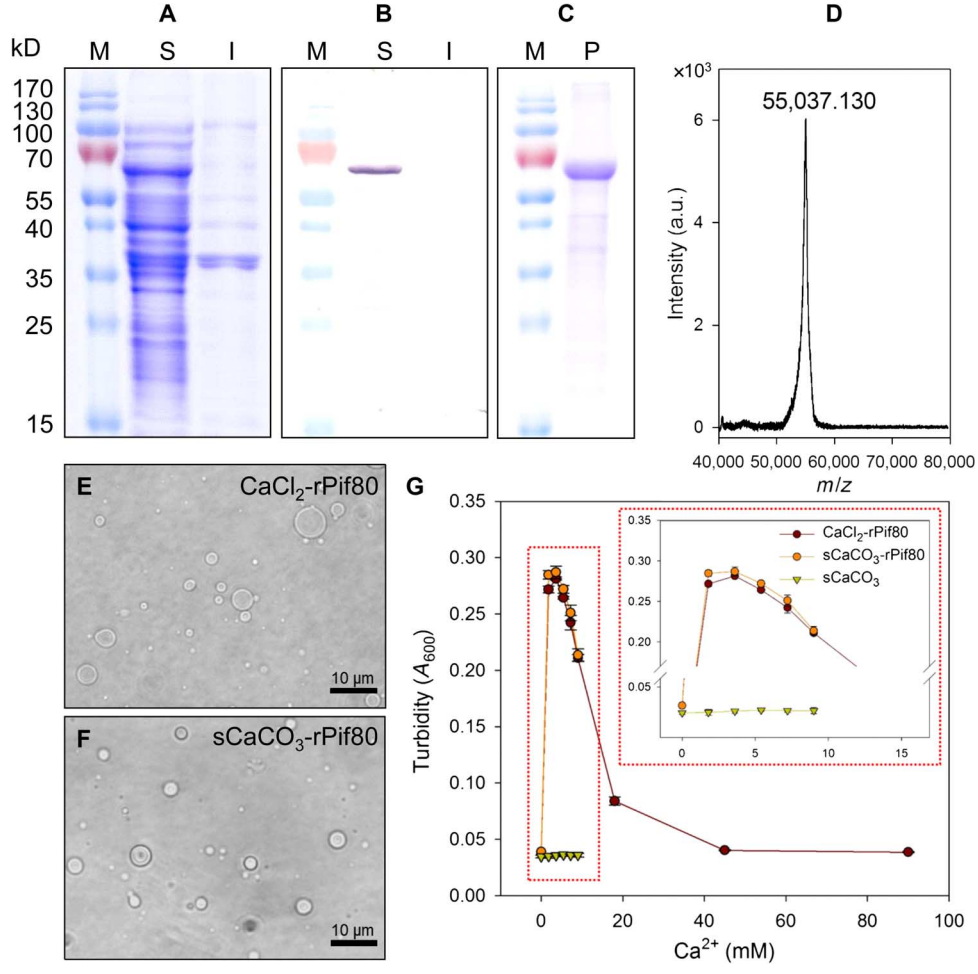

Fig. 1. Bacterial production and Ca^{2+}-induced coacervation of rPif80. (**A** to **C**) Analyses of expressed rPif80 in *E. coli* by SDS-PAGE with Coomassie staining (A), Western blot detection of the His_6 tag in cell lysate (B), and purified rPif80 by SDS-PAGE with Coomassie staining (C). Lanes: M, protein molecular weight marker; S, soluble fraction; I, insoluble fraction; P, purified rPif80. (**D**) MALDI-TOF MS analysis of purified rPif80. a.u., arbitrary units. (**E** and **F**) Optical micrograph of the coacervate droplets of rPif80 in solutions of $CaCl_2$ (E) and supersaturated $CaCO_3$ (F). (**G**) Turbidimetric measurements of rPif80 coacervation according to Ca^{2+} concentration in solutions of $CaCl_2$ and supersaturated $CaCO_3$. Turbidity of the supersaturated $CaCO_3$ solution in the absence of rPif80 was measured to exclude the possible influence of mineral growth on the increase of turbidity. All of the measurements were performed in triplicate. $CaCl_2$-rPif80, coacervation of rPif80 in $CaCl_2$ solution; $sCaCO_3$-rPif80, coacervation of rPif80 in supersaturated $CaCO_3$ solution; $sCaCO_3$, supersaturated $CaCO_3$ solution.

mollusks (fig. S2A) (*23*, *24*). The rPif80 coacervation mainly occurred at Ca^{2+} concentrations below 10 mM, peaking at a concentration of approximately 4 mM (Fig. 1G), and the formation of rPif80 coacervates was directly proportional to the concentration of rPif80 (fig. S2B). The interaction of Pif80 with Ca^{2+} was expected because of its high content of acidic residues. Stains-All staining of rPif80 revealed a blue band, indicating the potential Ca^{2+}-binding property of rPif80, whereas bovine serum albumin (BSA) with a similar acidity (pI = 4.7) (*25*) was negatively stained (pink color) (fig. S3). Thus, the acidic nature alone might be insufficient for rPif80 to interact with Ca^{2+}, and the specific primary structure, including intrinsic disorder and aggregation-prone sequences, appears to be a more important factor (*19*, *26*). The formation of rPif80 coacervates was inhibited by increasing the concentration of additional salts such as NaCl (fig. S2C). Similarly, preformed coacervates were broken up by treatment with additional salts (fig. S4). Collectively, these results indicate that the coacervation of rPif80 can be achieved by the addition of Ca^{2+} under salt-deficient physiological pH conditions and that the Ca^{2+}-induced rPif80 coacervates (Ca^{2+}-rPif80 coacervates) can be broken up upon exposure to the extrapallial fluid or seawater that contain high salt contents. In addition, these behaviors support the idea that electrostatic interaction is the major driving force for the coacervation of Pif80 via self-charge neutralization induced by interaction with Ca^{2+}.

Stabilization of polymer-induced liquid precursor–like amorphous $CaCO_3$ granules by Ca^{2+}-rPif80 coacervates

Mineralization of $CaCO_3$ was performed by mixing a CO_3^{2-}/HCO_3^- solution with Ca^{2+} in the presence or absence of rPif80 (pH ~8.8). In the absence of rPif80, $CaCO_3$ precipitates were immediately formed and transformed to thermodynamically stable crystalline calcite within 2 hours at 4°C, as confirmed by Raman spectroscopic analysis (fig. S5A). In the presence of rPif80, the rPif80-induced condensed liquid-like phase (rPif80-CLP) was found in droplet form (Fig. 2A). When analyzed using cryo–transmission electron microscopy (cryo-TEM), the droplets were composed mainly of a large amount of electron-dense granules with a size of less than tens of nanometers (Fig. 2B). It was reasonable to assume that the granules consisted of mineral $CaCO_3$ considering their electron density. The distribution of granules seemed to correspond to that of calcium in an energy-dispersive x-ray spectroscopy (EDS) analysis, which also supports the idea that the granules are formed from a calcium mineral compound (fig. S6). Considering the fluidic characteristics, the $CaCO_3$ granules could be regarded as a polymer-induced liquid precursor (PILP)–like phase, whose formation has been suggested as a mineral regulation process in nonclassical nucleation pathway (*26*, *27*). Ca^{2+}-rPif80 coacervates were stable under moderately basic conditions with a relatively low concentration of salts, suggesting that the Ca^{2+}-rPif80 coacervates and PILP-like $CaCO_3$ granules can coexist, resulting in an rPif80-CLP. The granules were observed only inside the rPif80-CLP and showed no electron diffraction pattern (Fig. 2C). In Raman analysis, only the ν_1 vibration mode peak of $CaCO_3$ was observed (Fig. 2D), which is similar to the relatively broad peak from the Raman spectra of stable biogenic amorphous $CaCO_3$ (*13*, *28*). These results indicate that the PILP-like granules are actually an amorphous phase of $CaCO_3$. Although amorphous $CaCO_3$ is the least stable phase among $CaCO_3$ polymorphs, PILP-like amorphous $CaCO_3$ granules (PILP-like ACGs) were highly stabilized in the rPif80-CLP. Remarkably, this amorphous property was maintained even after a 4-day incubation at 4°C; no change was observed in either the electron diffraction pattern or the Raman spectrum (Fig. 2, C and D). This stabilization could not be achieved using other conventional coacervates such as the lysozyme–hyaluronic acid (HA) complex, which showed immediate calcite growth (fig. S5B). Therefore, the stabilization effect on

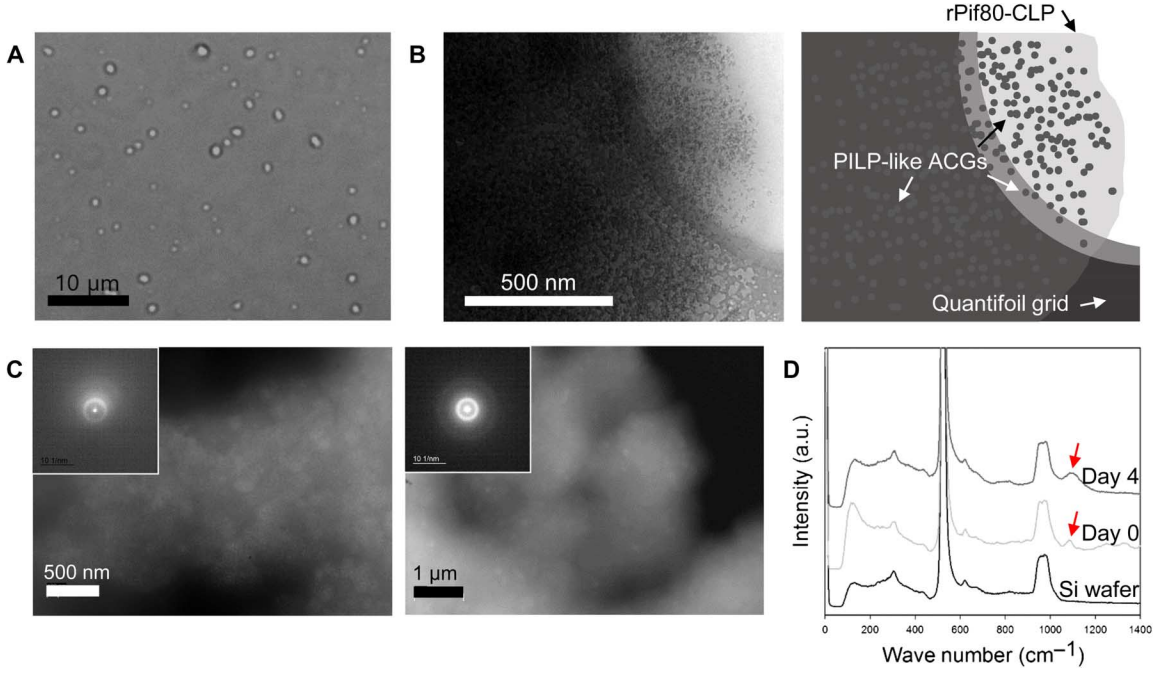

Fig. 2. rPif80-induced CLP. (**A**) Optical micrograph of rPif80-CLP droplets in the presence of Ca^{2+} and CO_3^{2-}/HCO_3^-. (**B**) Cryo-TEM image (left) and illustration (right) of rPif80-CLP droplets in (A). Dense granules of PILP-like ACGs are shown inside rPif80-CLP with cloudy morphology. (**C**) Cryo-scanning TEM image and electron diffraction pattern (inset) of rPif80-CLP droplets after initial formation (left) and a 4-day incubation at 4°C (right). (**D**) Raman spectra of the rPif80-CLP after initial formation and a 4-day incubation at 4°C. The Raman spectrum of an Si wafer is presented for comparison. The red arrows indicate the ν_1 vibration mode of $CaCO_3$.

PILP-like ACGs, evenunder aqueous condition, is a distinctive feature of Ca^{2+}-rPif80 coacervates.

Plate aragonite formation on chitin surface by rPif80

Pif80 has been suggested to act as a framework protein in aragonite crystallization (*19*). As expected, rPif80 has aragonite-binding ability, which is consistent with that of the native form (fig. S7). In in vitro $CaCO_3$ crystallization, β-chitin, the major organic matrix of nacre, was used as a template, and a $CaCO_3$ solution was applied to slowly crystallize $CaCO_3$ by the diffusion of dissolved carbon dioxide (CO_2). To mimic the nacre formation conditions, we prepared a biomimetic crystallization solution by adding 50 mM $MgCl_2$ and 500 mM NaCl to the $CaCO_3$ solution, which corresponds to the major inorganic composition of extrapallial fluid (*24*). In this solution, the Ca^{2+}-rPif80 coacervates could not be formed because of the high salt concentration, as mentioned above. A scanning electron microscopy (SEM) analysis showed that the biomimetic crystallization solution induced twinned spherical-shaped minerals on the β-chitin surface after a 48-hour incubation at 20°C when rPif80 was absent (Fig. 3A); these minerals were confirmed to be aragonites by Raman analysis (Fig. 3G). However, rPif80 induced the growth of minerals with different morphologies, that is, flat edges and hemispherical centers (Fig. 3, B and C). Both polymorphs of the edge and the center were confirmed to be aragonites (Fig. 3G). The flat region was gradually extended from the edge to the center of the minerals, with increase of the rPif80 concentration to 50 μg/ml (Fig. 3, B to D). In the presence of rPif80 (50 μg/ml), the entire aragonite was flattened, showing a circular plate morphology (Fig. 3, D and G). A cross section of the plate mineral was prepared

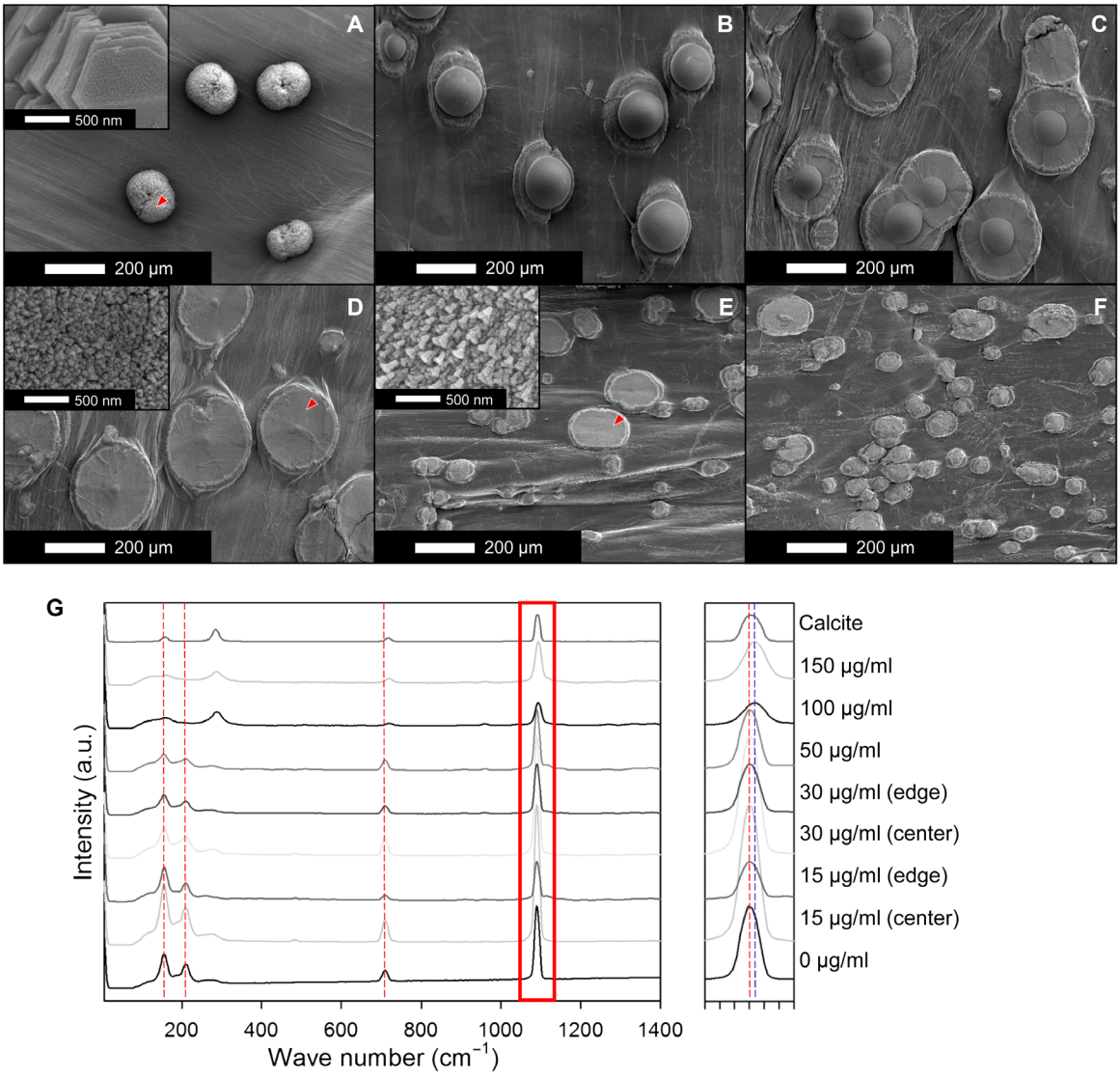

Fig. 3. Morphology and polymorph analyses of grown minerals obtained by in vitro $CaCO_3$ crystallization on β-chitin. (**A** to **F**) SEM images of grown minerals after crystallization at 20°C for 48 hours in the presence of rPif80 at concentrations of 0 (A), 15 (B), 30 (C), 50 (D), 100 (E), and 150 μg/ml (F). The insets of (A), (D), and (E) are magnified images of the selected areas indicated by the red arrowheads. (**G**) Raman spectra of grown minerals in (A) to (F) (left), and enlarged spectra from the red box (right). The Raman spectrum of calcite powder is presented for comparison. The red dashed lines correspond to the Raman peaks of aragonite, and the blue dashed line indicates the shift in the ν_1 vibration mode of $CaCO_3$.

with a focused ion beam (FIB), and the inner structure was analyzed by TEM (fig. S8, A to C). The selected area electron diffraction pattern of the cross section corresponded to the aragonite (fig. S8B). However, high-resolution TEM (HR-TEM) with fast Fourier transform patterns showed that the inner structure also contained misoriented and less crystalline nanocrystals (fig. S8C). The aragonites obtained in the presence of rPif80 were composed of spherical aragonite nanogranules that were tens of nanometers in size (inset in Fig. 3D), whereas twinned spherical aragonites obtained in the absence of rPif80 showed hexagonal tablet tiling (inset in Fig. 3A). rPif80 concentrations greater than 100 μg/ml generated minerals with irregular morphology and smaller size than those of plate aragonites (Fig. 3, E and F); these minerals were confirmed to be magnesian calcite by Raman analysis, with a slight shift of spectra with respect to that of calcite (Fig. 3G). The magnesian calcite showed a typical trigonal nanostructure (inset in Fig. 3E) (*29*). The host cell protein impurities did not contribute to the morphology of aragonite, indicating that rPif80 was responsible for the unique morphology control (fig. S9).

The concentration of proteins in extrapallial fluid of *P. fucata* has been found to be about 0.2 to 0.4 mg/ml (*30*). Considering that the extrapallial fluid contains several different proteins, a Pif80 concentration of 50 μg/ml seems to be realistic under in situ conditions. However, because the exact physiological conditions of mineralization sites may be different from those in our experiments, the optimal concentration of Pif80 under in situ conditions might be somewhat different from that obtained in our experiments. Nevertheless, it seems that Pif80 optimally controls the aragonite morphology at a particular concentration. Moreover, an excess of protein inhibits $CaCO_3$ crystallization, resulting in the irregular growth of a thermodynamically stable calcite that, unlike aragonite, has lattice positions available for the incorporation of magnesium (*29*).

DISCUSSION

Nacre biomineralization is a process conducted by mollusks and uses organic matrices to develop highly organized aragonite $CaCO_3$ from Ca^{2+}. Direct mineralization of aragonite tablets on calcification sites from a saturated $CaCO_3$ solution is logistically insufficient, suggesting that an initial mineral phase is formed elsewhere and transported to the calcification site (*7*). Vesicles containing amorphous phase $CaCO_3$, a transient precursor of the crystalline phase of the nacreous layer, have been observed in tissues of mollusks, suggesting that these specialized intracellular vesicles can be regarded as a transient mineral deposition area (*9*, *10*, *31*). However, how this highly unstable amorphous $CaCO_3$ is maintained in the vesicle is poorly understood because of the difficulty of investigating cellular environments, although membrane lipids (*32*), Mg^{2+} (*33*), and/or organic macromolecules (*34*–*36*) seem to be involved in the stabilization of the disordered phase of $CaCO_3$.

This study suggests a process for effective Ca^{2+} capture and mineral precursor stabilization in mantle cells using the coacervate phase; this phase is also involved in special functions of marine organisms, such as sandcastle worms (*37*), mussels (*38*), and squids (*39*), in their aqueous environments. Although the glue of sandcastle worms shows typical polycation/polyanion complex coacervation (*37*), other mechanisms such as hydrophobic interaction and balanced force of both electrostatic and hydrophobic interactions have been suggested for simple coacervation of mussel and squid proteins, respectively (*38*, *39*). On the other hand, rPif80 seems to undergo electrostatically driven simple coacervation on the basis of characteristics such as the high proportion of well-balanced charged amino acid residues and induction of phase separation by interaction with Ca^{2+}. The salt dependence also supports the electrostatically driven coacervation.

We hypothesized that the optimal Ca^{2+} concentration for efficient rPif80 coacervation (4 mM) (Fig. 1G) is lower than that of the body fluids of marine organisms (approximately 10 mM) (*24*), because intracellular Ca^{2+} is not only used for coacervation but also consumed in the formation of the initial mineral phase in mantle vesicles. Our results suggest that the CLP, composed of PILP-like ACGs and Ca^{2+}-rPif80 coacervates, can be formed in moderately basic conditions with a relatively low concentration of salts compared to that of seawater and that the PILP-like ACGs are highly stabilized under these conditions (Fig. 2). The required conditions for stabilizing PILP-like ACGs seem to arise from the inherent properties of both rPif80 itself and its coacervate phase, because other conventional coacervates did not inhibit transformation to crystalline $CaCO_3$ (fig. S5B) and disruption of Ca^{2+}-rPif80 coacervates also resulted in growth of the crystalline phase (Fig. 3). In mantle cells, Pif80 might play roles both as an inducer of PILP-like ACGs and as a stabilizing agent of PILP-like ACGs in the form of Ca^{2+}-induced Pif80 coacervates, which can be reversibly regulated by pH and salt conditions. The elevated pH of intracellular vesicles compared to the surrounding intracellular environment can provide appropriate conditions for preparing the mineral precursor phase (*23*).

We also suggest that destabilization of the PILP-like ACGs is induced by the disruption of Ca^{2+}-induced Pif80 coacervates, and their transformation into crystalline aragonite is controlled by redissolved Pif80. The shear-thinning viscosity of coacervates (*40*) is suitable for the secretion of PILP-like ACGs from mantle vesicles to the extrapallial space via narrow openings generated during exocytosis. The high concentration of ionic salts in the extrapallial fluid breaks the rPif80 coacervates, and the PILP-like ACGs are consequently destabilized and act as a precursor to nacreous aragonite. The concomitantly redissolved rPif80 contributes to the growth of the aragonite plate shape on the chitin template (Fig. 3D), which can be regarded as the result of the lateral growth of minerals from the center. Despite the differences in their sizes, the plate morphology seemed similar to that of incipient aragonite platelets identified in the nacreous layers of *Pinctada* species (*41*, *42*). In addition, plate morphology has been proposed to be a nascent shape of mature polygonal aragonite tablets of nacre, produced by lateral extension until contact with adjacent tablets (*7*, *41*). In nature, Pif80 may play a role in controlled mineralization to produce polygonal aragonite tablets of nacre in combination with β-chitin matrix and neighboring nucleation sites. Pif80 has yet to be located adjacent to tablets, interacting with mineral aragonite. Considering that the growth of $CaCO_3$ with similar plate morphologies was observed in the presence of polysaccharide templates with acidic polypeptides (*43*) or poly(acrylic acid) (*44*), the acidic amino acid residue cluster in Pif80 may also have an important function in the regulation of crystal growth. In addition, the aggregated nanogranule structure constituting the plate aragonite induced by rPif80 appeared to be comparable to the nanostructure of molluscan nacre, which is regarded as an important factor in the toughening of nacre (*45*, *46*). However, the plate aragonite in our study was not in the single crystalline form that is a distinctive feature of nacreous aragonite tablets. It has been suggested that single crystals experience amorphous and polycrystalline states in crystallization (*47*). We believe that the polycrystalline and less crystalline structure of plate aragonite produced in the presence of rPif80 reflects a still-maturing crystalline phase, because the polycrystalline structure appeared to be similar to the misoriented

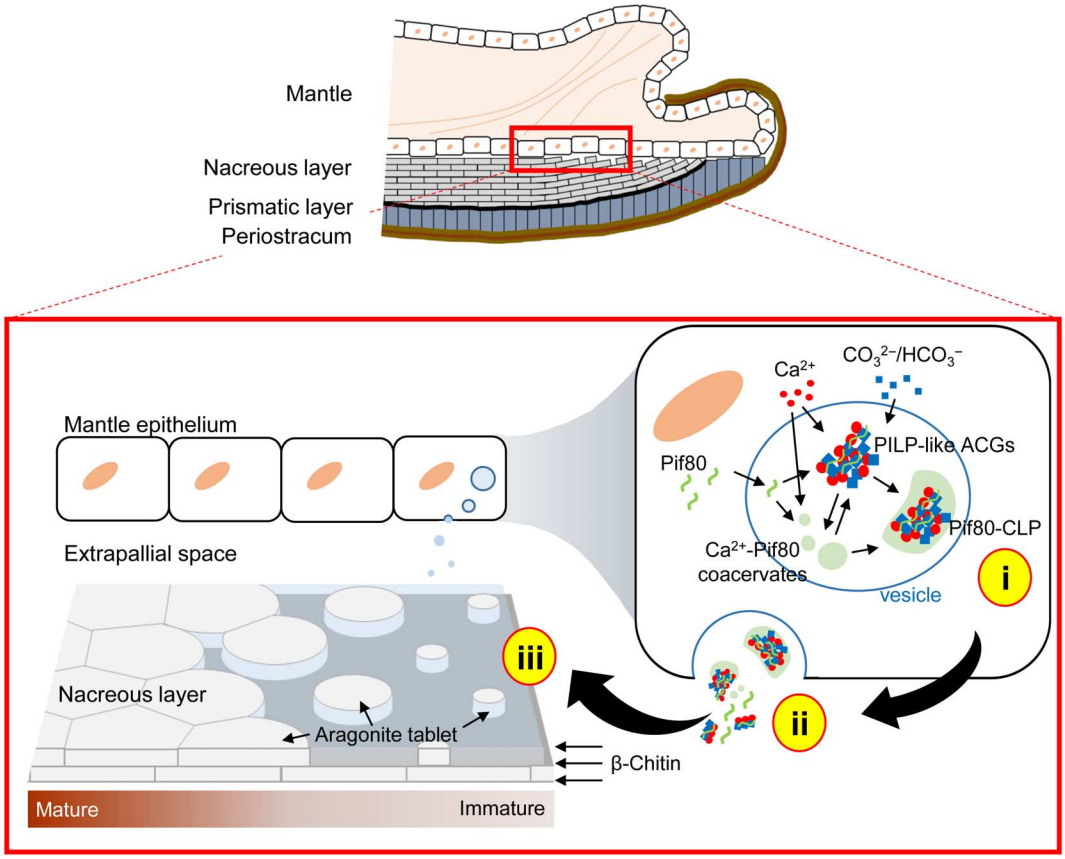

Fig. 4. Schematic illustration of the proposed roles of Pif80 in the nacre formation in *P. fucata*. Nacre formation is processed through the following steps: (i) PILP-like ACGs are formed in intracellular vesicles and stably stored as a form of Pif80-CLP by a Ca^{2+}-Pif80 coacervate. (ii) The PILP-like ACGs are destabilized by the disruption of the Ca^{2+}-Pif80 coacervate in the extrapallial space and supplied for crystallization of nacre. (iii) Nacreous aragonites are grown on the β-chitin substrate using redissolved Pif80, eventually leading to the maturation of polygonal tablets.

nanocrystalline structure observed in immature nacre tablets (*48*). Further maturation and co-orientation of nanocrystals may require the cooperation of other macromolecular components of the Pif complex such as Pif97 and N16, which have been shown to contribute to oriented aragonite formation (*15*).

In summary, the following functional aspects of Pif80 are thought to be involved in the nacre formation pathway: (i) formation and storage of the initial mineral phase, (ii) secretion of the mineral to the extrapallial space, and (iii) the growth of aragonite tablets (Fig. 4). In the first stage, mantle epithelial cells uptake Ca^{2+} and CO_3^{2-}/HCO_3^- from the extracellular fluid and transport them to internal vesicles, in which Ca^{2+}-Pif80 coacervates and PILP-like ACGs are formed under balanced pH and salt concentrations, resulting in the formation of a Pif80-CLP. The PILP-like ACGs are stabilized by coacervates and stored until required. The amorphous minerals are then transported from the vesicles to the site of mineralization by exocytosis. Coacervates offer a favorable characteristic for the secretion at a narrow opening, and the PILP-like ACGs are transported to the extrapallial space. The high salt concentration of the extrapallial fluid disrupts the Ca^{2+}-induced Pif80 coacervates, and the PILP-like ACGs are subsequently released and destabilized for crystal formation. Simultaneously, Pif80 is redissolved to control the transformation of the amorphous mineral precursor. Finally, crystallization proceeds via the supplied mineral precursors, and the redissolved Pif80 controls the growth of aragonite, contributing to the polygonal morphology of the nacre aragonite tablets. From a biological point of view, the proposed mechanism of nacre formation offers a new perspective on the stepwise flow of Ca^{2+} from an ionic state to a specialized biomineral via an amorphous precursor. These results provide insight into how living organisms use organic macromolecules to control the development of inorganics in biomineralization pathways, which can be exploited for the production of biomimetic materials, including stabilized amorphous $CaCO_3$ and nacre-like aragonites from an engineering perspective.

MATERIALS AND METHODS

Vector construction

The protein sequence of *P. fucata* Pif80 was obtained from the work of Suzuki *et al.* (*15*). The gene encoding Pif80 was optimized for protein expression by adjusting the codon usage and frequency to match the preferences of *E. coli*. The target gene was constructed with the addition of N-terminal Nde I and C-terminal Xho I restriction sites (GenScript USA Inc.) and was inserted into a pET-22b(+) vector (Novagen), resulting in pET22-rPif80. The amino acid sequence of rPif80 was expected to be identical to that of native Pif80, except for an additional N-terminal methionine (from the start codon) and eight amino acids at the C terminus (LEHHHHHH; two from an Xho I restriction site and six from a His_6 tag). *E. coli* TOP10 (Invitrogen) was transformed by the constructed plasmid and cultured in Luria-Bertani (LB) medium supplemented with ampicillin (50 μg/ml) (Sigma-Aldrich). The gene

sequence of the constructed pET22-rPif80 vector was confirmed by direct sequencing.

Production and purification of rPif80

The recombinant plasmid pET22-rPif80 was introduced to *E. coli* BL21 (DE3) (Novagen) for the expression of rPif80. The recombinant cells were cultured in 400 ml of LB medium supplemented with ampicillin (50 μg/ml) at 37°C and 200 rpm in a shaking incubator. The expression of rPif80 was induced by 100 μM isopropyl-β-D-thiogalactopyranoside (Sigma-Aldrich) when the cell density (optical density at 600 nm) reached 0.8 to 1.0 and further incubated at 20°C for 20 hours. The cells were harvested by centrifugation at 4°C and 4000*g* for 10 min. For expression check, the cell pellet was resuspended with 40 ml of lysis buffer [50 mM NaH_2PO_4 and 300 mM NaCl (pH 8)] and disrupted using a sonic dismembrator (Sonics & Materials Inc.) at 30% power with a 3-s pulse on and 7-s pulse off repetition cycle on ice. The lysate was fractionated by centrifugation at 4°C and 10,000*g* for 20 min. The supernatant and the resultant pellet were designated as the soluble and insoluble fractions, respectively.

For protein purification, the cell pellet was resuspended with 40 ml of denaturing lysis buffer [100 mM NaH_2PO_4, 10 mM tris, and 8 M urea (pH 8)]. The cells were disrupted, the lysate was fractionated by centrifugation at 4°C and 10,000*g* for 20 min, and the supernatant was used for rPif80 purification. The supernatant was mixed with Ni-nitrilotriacetic acid resin (Qiagen), and the mixture was agitated for 1 hour to allow the target protein to bind the resin. After washing the resin by wash buffer [100 mM NaH_2PO_4, 10 mM tris, 8 M urea, and 20 mM imidazole (pH 8)], rPif80 was eluted using elution buffer [100 mM NaH_2PO_4, 10 mM tris, 8 M urea, and 200 mM imidazole (pH 8)]. The eluate was concentrated by ultrafiltration (Amicon Ultra, EMD Millipore) and further purified by fast protein liquid chromatography (ÄKTA FPLC, GE Healthcare) with a HiPrep 26/60 Sephacryl S-200 HR column (GE Healthcare). Sample was separated using isocratic method in phosphate buffer [50 mM NaH_2PO_4 and 300 mM NaCl (pH 8)] and was monitored by measuring the absorbance at 280 nm. The target fraction was concentrated by ultrafiltration and desalted using a PD-10 column (GE Healthcare) with 10 mM tris buffer (pH 8) and stored at 4°C for further analyses. For control experiment, the host cell protein impurities were separately prepared via His_6 tag affinity chromatography by using cleared cell lysate from *E. coli* BL21 (DE3) containing the parent vector pET-22b(+). The eluted proteins were concentrated by ultrafiltration and desalted using the PD-10 column with 10 mM tris buffer (pH 8).

MS analysis

The molecular weight of the purified rPif80 was confirmed by MALDI-TOF MS (autoflex speed LRF, Bruker Daltonics). The protein sample was diluted with 50% acetonitrile and 0.3% trifluoroacetic acid and analyzed using the α-cyano-4-hydroxycinnamic acid matrix.

SDS-PAGE and Western blot analyses

For SDS-PAGE analysis, the sample buffer [50 mM tris, 2% SDS, 10% glycerol, 1% β-mercaptoethanol, and 0.004% bromophenol blue (pH 6.8)] was mixed with each sample, and the mixture was boiled at 100°C for 10 min. After the proteins were separated on a 15% SDS-polyacrylamide gel according to the standard protocol, the gel was stained with Coomassie Blue R-250 (Bio-Rad). The intensity of the target band was evaluated by ImageJ software (National Institutes of Health; imagej.nih.gov/ij/). For the Western blot analysis, the proteins separated by SDS-PAGE were transferred to a nitrocellulose membrane (Thermo Fisher Scientific). After the membrane was sequentially treated with a primary monoclonal anti-His_6 antibody (abm) and a secondary anti-mouse immunoglobulin G alkaline phosphatase–conjugated antibody (Sigma-Aldrich), the target protein containing a His_6 tag was visualized with a color development reaction using nitro blue tetrazolium (Bio Basic) and 5-bromo-4-chloro-3-indolyl phosphate (Bio Basic).

Organic matrix extraction from nacre

The acid-insoluble and SDS-soluble organic matrix of nacre (AIM), including the Pif complex, was extracted on the basis of a previously described method (*15*). In brief, after dissolution of the mineral phase of dried *P. fucata* shells by treatment with 1 M acetic acid, the AIM of the nacreous layer was extracted by boiling the sample at 100°C for 10 min in extraction buffer [50 mM tris, 1% SDS, and 10 mM dithiothreitol (pH 8)].

Gel staining assay

To identify glycosylation and phosphorylation of native Pif80, periodic acid–Schiff staining (Thermo Fisher Scientific) and Pro-Q Diamond staining (Invitrogen) were performed after SDS-PAGE according to the manufacturer's instructions. For the Stains-All staining, BSA (Promega) was used as a negative control. The Stains-All staining was performed on the basis of a previously described method (*49*). The SDS-PAGE gel was washed twice in 25% isopropanol (Duksan) to remove the SDS and was fixed overnight with 25% isopropanol. The gel was soaked in fresh Stains-All staining solution [15 mM tris, 0.005% Stains-All (Sigma-Aldrich), 10% formamide (Merck Millipore), and 25% isopropanol (pH 8.8)] for 24 hours in dark conditions at room temperature with gentle agitation. After the gel was washed with distilled water (DW) several times, it was scanned using a gel scanner.

Ca^{2+}-induced coacervation of rPif80 and turbidimetric measurement

Ca^{2+} solutions were prepared for the induction of rPif80 coacervation. A $CaCl_2$ aqueous solution was prepared by dissolving $CaCl_2$ powder (Sigma-Aldrich) in DW. To prepare the supersaturated $CaCO_3$ solution (in which ions existed in the form of Ca^{2+} and HCO_3^- at early stage), CO_2 gas was bubbled through $CaCO_3$ powder (Sigma-Aldrich) containing DW (2 g/liter) at 4°C for 3 hours. The undissolved solid $CaCO_3$ was removed using a 0.2-μm filter (Sartorius Stedim Biotech), and the remaining aqueous solution was kept at 4°C with CO_2 bubbling until use. The Ca^{2+} concentration of the supersaturated $CaCO_3$ solution was measured with QuantiChrom Calcium Assay Kit (BioAssay Systems). For morphology observation, an rPif80 solution (3 g/liter) was mixed with a 6 mM Ca^{2+} solution at a ratio of 1:1 (v/v). After 10 min at room temperature, coacervate droplets were observed by phase-contrast optical microscopy (BX60, Olympus).

For the turbidity measurements, Ca^{2+} solutions of various concentrations were directly mixed with the rPif80 solution (3 g/liter) at a ratio of 9:1 (v/v). Mixtures of a supersaturated $CaCO_3$ solution and 10 mM tris (pH 8) at the same ratio were prepared to exclude any pH effect on turbidity. The turbidity values at different pH values were measured in 4 mM $CaCl_2$ with 20 mM tris (pH 7 to 9). The effect of NaCl on coacervation was examined in 4 mM $CaCl_2$ and 20 mM tris (pH 8), with a range of NaCl (Samchun) concentrations up to 200 mM. They were incubated at room temperature for 10 min before the measurement. To examine the effect of NaCl on dissolution of Ca^{2+}-rPif80 coacervates, the preformed coacervate was treated with a range of NaCl concentrations up to 500 mM. The samples were transferred to a flat-bottom 96-well plate (SPL Life Sciences),

and the absorbance was measured at 600 nm using a microplate spectrophotometer (Bio-Rad). The turbidimetric experiments were performed in triplicate.

PILP-like amorphous $CaCO_3$ formation using rPif80

$CaCl_2$, Na_2CO_3 (Sigma), and $NaHCO_3$ (Sigma) powders were dissolved in 10 mM tris (pH 8) and used for $CaCO_3$ mineralization at a final concentration of 10, 8, and 2 mM, respectively. The measured pH of the resulting mineralization solution was approximately 8.8. For simultaneous mineralization and coacervation, rPif80 was homogeneously mixed with Na_2CO_3/$NaHCO_3$ solutions, and then, the $CaCl_2$ solution was added to the mixture. The final concentration of rPif80 was 1 g/liter. Control experiments were performed without rPif80 or with lysozyme-HA complex coacervate (*50*). For complex coacervation, lysozyme and HA were used at concentrations of 3 and 1 g/liter, respectively. After the reaction, the samples were incubated at 4°C for further analysis.

The resulting CLP was observed by phase-contrast optical microscopy, and grown mineral precipitates on an Si wafer were observed by optical microscopy (CK30, Olympus) and analyzed by confocal Raman microscopy (alpha300 RA Plus, WITec) to determine the polymorph of the mineral. To investigate the inside of the liquid phase, aliquots of the suspensions were blotted on a grid and quickly frozen for microscopic analysis, electron diffraction patterns, and EDS performed with cryo-TEM (Libra 200 HT MC Cs, Carl Zeiss), using a Gatan 626 cryo transfer holder (Gatan) and operating at approximately −180°C.

$CaCO_3$-binding assay

Commercially available calcite powder (Sigma-Aldrich) was used for the mineral-binding assay. Aragonite powder was manufactured according to previous studies (*18*). In brief, 50 mM $Ca(OH)_2$ powder (Sigma-Aldrich) suspended in a 150 mM $MgCl_2$ solution was heated to 70°C, with bubbling CO_2 gas. After a constant pH was established, the solution was filtered, and the slurry was washed with ethanol (Merck Millipore) and DW. After the powder was dried, the crystal phase of the aragonite was confirmed by x-ray diffraction (D/Max-2500/PC, Rigaku) and field-emission SEM (FE-SEM) (XL30S FEG, Philips Electron Optics B.V.).

For the binding assay, 10 mg of $CaCO_3$ powder was mixed with 50 μl of protein solution (0.5 g/liter), and the mixture was incubated at 20°C for 16 hours with vigorous shaking. After centrifugation, the supernatant was removed and designated as flow-through, and the resulting $CaCO_3$ pellet was sequentially washed with 50 μl of 10 mM tris buffer (pH 8) and the same buffer supplemented with 0.1 M NaCl and 0.5 M NaCl. Finally, the remaining $CaCO_3$ pellet was dissolved in the same volume of 4 M acetic acid. The protein contents were analyzed by dot blotting on a nitrocellulose membrane, followed by Coomassie Blue staining.

In vitro $CaCO_3$ crystallization

β-Chitin was prepared from the pens of *Loligo* species and was used as a mineralization template after purification by treatment with a 1 M NaOH solution at 4°C for 3 days with stirring; the solution was changed once per day (*12*, *51*). Following extensive washing with DW, the β-chitin was stored dry. The mineralization solution was prepared using a supersaturated $CaCO_3$ solution with the addition of 50 mM $MgCl_2$, 500 mM NaCl, and rPif80 at varying concentrations. The final Ca^{2+} concentration for the mineralization solution was 9.7 mM. $CaCO_3$ mineralization was performed in a 96-well plate by soaking β-chitin substrates in the mineralization solution. After being incubated at 20°C for 48 hours, the substrates with mineralized $CaCO_3$ were rinsed with DW and dried for the analyses. The morphology of $CaCO_3$ was observed by FE-SEM, and the polymorph was confirmed by confocal Raman microscopy. The cross section of the mineral was obtained by an FIB system and analyzed by HR-TEM (JEM-2200FS, JEOL).

SUPPLEMENTARY MATERIALS

Supplementary material for this article is available at http://advances.sciencemag.org/cgi/content/full/3/8/e1700765/DC1

fig. S1. PTM analyses of native Pif80.
fig. S2. Turbidimetric measurement of Ca^{2+}-induced coacervation of rPif80 in the presence of 4 mM $CaCl_2$.
fig. S3. SDS-PAGE analysis with Stains-All staining of rPif80.
fig. S4. Turbidimetric measurement of Ca^{2+}-rPif80 coacervates according to additional NaCl.
fig. S5. Optical micrograph images (top) and Raman spectra (bottom) of mineralized $CaCO_3$.
fig. S6. Cryo-scanning TEM image and EDS mapping analyses of rPif80-CLP.
fig. S7. Dot blotting with Coomassie staining after $CaCO_3$-binding analysis of rPif80.
fig. S8. Structural analyses of a cross-sectioned plate mineral induced by rPif80 at a concentration of 50 μg/ml.
fig. S9. Morphology and polymorph analyses of grown minerals in the presence of protein impurities.

REFERENCES AND NOTES

1. J. Sun, B. Bhushan, Hierarchical structure and mechanical properties of nacre: A review. *RSC Adv.* **2**, 7617–7632 (2012).
2. F. Barthelat, Biomimetics for next generation materials. *Philos. Trans. A Math. Phys. Eng. Sci.* **365**, 2907–2919 (2007).
3. J. D. Currey, Mechanical properties of mother of pearl in tension. *Proc. R. Soc. Lond. B Biol. Sci.* **196**, 443–463 (1977).
4. G. M. Luz, J. F. Mano, Biomimetic design of materials and biomaterials inspired by the structure of nacre. *Philos. Trans. A Math. Phys. Eng. Sci.* **367**, 1587–1605 (2009).
5. F. Marin, N. Le Roy, B. Marie, The formation and mineralization of mollusk shell. *Front. Biosci. Scholar Ed.* **4**, 1099–1125 (2012).
6. F. Marin, G. Luquet, B. Marie, D. Medakovic, Molluscan shell proteins: Primary structure, origin, and evolution. *Curr. Top. Dev. Biol.* **80**, 209–276 (2007).
7. L. Addadi, D. Joester, F. Nudelman, S. Weiner, Mollusk shell formation: A source of new concepts for understanding biomineralization processes. *Chem. Eur. J.* **12**, 980–987 (2006).
8. B. Marie, C. Joubert, A. Tayalé, I. Zanella-Cléon, C. Belliard, D. Piquemal, N. Cochennec-Laureau, F. Marin, Y. Gueguen, C. Montagnani, Different secretory repertoires control the biomineralization processes of prism and nacre deposition of the pearl oyster shell. *Proc. Natl. Acad. Sci. U.S.A.* **109**, 20986–20991 (2012).
9. J. M. Neff, Ultrastructure of the outer epithelium of the mantle in the clam *Mercenaria mercenaria* in relation to calcification of the shell. *Tissue Cell* **4**, 591–600 (1972).
10. S. Weiner, L. Addadi, Crystallization pathways in biomineralization. *Annu. Rev. Mater. Res.* **41**, 21–40 (2011).
11. A. M. Belcher, X. H. Wu, R. J. Christensen, P. K. Hansma, G. D. Stucky, D. E. Morse, Control of crystal phase switching and orientation by soluble mollusc-shell proteins. *Nature* **381**, 56–58 (1996).
12. G. Falini, S. Albeck, S. Weiner, L. Addadi, Control of aragonite or calcite polymorphism by mollusk shell macromolecules. *Science* **271**, 67–69 (1996).
13. B.-A. Gotliv, L. Addadi, S. Weiner, Mollusk shell acidic proteins: In search of individual functions. *ChemBioChem* **4**, 522–529 (2003).
14. Z. Ma, J. Huang, J. Sun, G. Wang, C. Li, L. Xie, R. Zhang, A novel extrapallial fluid protein controls the morphology of nacre lamellae in the pearl oyster, *Pinctada fucata*. *J. Biol. Chem.* **282**, 23253–23263 (2007).
15. M. Suzuki, K. Saruwatari, T. Kogure, Y. Yamamoto, T. Nishimura, T. Kato, H. Nagasawa, An acidic matrix protein, Pif, is a key macromolecule for nacre formation. *Science* **325**, 1388–1390 (2009).
16. R. A. Metzler, J. S. Evans, C. E. Killian, D. Zhou, T. H. Churchill, N. P. Appathurai, S. N. Coppersmith, P. U. P. A. Gilbert, Nacre protein fragment templates lamellar aragonite growth. *J. Am. Chem. Soc.* **132**, 6329–6334 (2010).
17. M. Suzuki, A. Iwashima, M. Kimura, T. Kogure, H. Nagasawa, The molecular evolution of the pif family proteins in various species of mollusks. *Mar. Biotechnol.* **15**, 145–158 (2013).
18. S. Y. Bahn, B. H. Jo, B. H. Hwang, Y. S. Choi, H. J. Cha, Role of Pif97 in nacre biomineralization: In vitro characterization of recombinant Pif97 as a framework protein for the association of organic–inorganic layers in nacre. *Cryst. Growth Des.* **15**, 3666–3673 (2015).

19. J. S. Evans, Aragonite-associated biomineralization proteins are disordered and contain interactive motifs. *Bioinformatics* **28**, 3182–3185 (2012).
20. A. Shirai, A. Matsuyama, Y. Yashiroda, A. Hashimoto, Y. Kawamura, R. Arai, Y. Komatsu, S. Horinouchi, M. Yoshida, Global analysis of gel mobility of proteins and its use in target identification. *J. Biol. Chem.* **283**, 10745–10752 (2008).
21. H. G. Bungenberg de Jong, H. R. Kruyt, Coacervation (partial miscibility in colloid systems). *Proc. K. Ned. Akad. Wet.* **32**, 849–856 (1929).
22. H. B. Bohidar, Coacervates: A novel state of soft matter—An overview. *J. Surf. Sci. Technol.* **24**, 105–124 (2008).
23. S. Bentov, C. Brownlee, J. Erez, The role of seawater endocytosis in the biomineralization process in calcareous foraminifera. *Proc. Natl. Acad. Sci. U.S.A.* **106**, 21500–21504 (2009).
24. M. A. Crenshaw, The inorganic composition of molluscan extrapallial fluid. *Biol. Bull.* **143**, 506–512 (1972).
25. S. Ge, K. Kojio, A. Takahara, T. Kajiyama, Bovine serum albumin adsorption onto immobilized organotrichlorosilane surface: Influence of the phase separation on protein adsorption patterns. *J. Biomater. Sci. Polym. Ed.* **9**, 131–150 (1998).
26. J. S. Evans, "Liquid-like" biomineralization protein assemblies: A key to the regulation of non-classical nucleation. *CrstEngComm* **15**, 8388–8394 (2013).
27. L. B. Gower, D. J. Odom, Deposition of calcium carbonate films by a polymer-induced liquid-precursor (PILP) process. *J. Cryst. Growth* **210**, 719–734 (2000).
28. U. Wehrmeister, D. E. Jacob, A. L. Soldati, N. Loges, T. Häger, W. Hofmeister, Amorphous, nanocrystalline and crystalline calcium carbonates in biological materials. *J. Raman Spectrosc.* **42**, 926–935 (2011).
29. S. Raz, S. Weiner, L. Addadi, Formation of high-magnesian calcites via an amorphous precursor phase: Possible biological implications. *Adv. Mater.* **12**, 38–42 (2000).
30. J. Xie, J. Liang, J. Sun, J. Gao, S. Zhang, Y. Liu, L. Xie, R. Zhang, Influence of the extrapallial fluid of *Pinctada fucata* on the crystallization of calcium carbonate and shell biomineralization. *Cryst. Growth Des.* **16**, 672–680 (2016).
31. J. H. E. Cartwright, A. G. Checa, The dynamics of nacre self-assembly. *J. R. Soc. Interface* **4**, 491–504 (2007).
32. C. C. Tester, R. E. Brock, C.-H. Wu, M. R. Krejci, S. Weigand, D. Joester, In vitro synthesis and stabilization of amorphous calcium carbonate (ACC) nanoparticles within liposomes. *CrstEngComm* **13**, 3975–3978 (2011).
33. Y. Politi, D. R. Batchelor, P. Zaslansky, B. F. Chmelka, J. C. Weaver, I. Sagi, S. Weiner, L. Addadi, Role of magnesium ion in the stabilization of biogenic amorphous calcium carbonate: A structure-function investigation. *Chem. Mater.* **22**, 161–166 (2010).
34. S. Bentov, S. Weil, L. Glazer, A. Sagi, A. Berman, Stabilization of amorphous calcium carbonate by phosphate rich organic matrix proteins and by single phosphoamino acids. *J. Struct. Biol.* **171**, 207–215 (2010).
35. D. J. Tobler, J. D. Rodriguez Blanco, K. Dideriksen, K. K. Sand, N. Bovet, L. G. Benning, S. L. S. Stipp, The effect of aspartic acid and glycine on amorphous calcium carbonate (ACC) structure, stability and crystallization. *Procedia Earth Planet. Sci.* **10**, 143–148 (2014).
36. S. Raz, P. C. Hamilton, F. H. Wilt, S. Weiner, L. Addadi, The transient phase of amorphous calcium carbonate in sea urchin larval spicules: The involvement of proteins and magnesium ions in its formation and stabilization. *Adv. Funct. Mater.* **13**, 480–486 (2003).
37. H. Zhao, C. Sun, R. J. Stewart, J. H. Waite, Cement proteins of the tube-building polychaete *Phragmatopoma californica*. *J. Biol. Chem.* **280**, 42938–42944 (2005).
38. W. Wei, Y. Tan, N. R. Martinez Rodriguez, J. Yu, J. N. Israelachvili, J. H. Waite, A mussel-derived one component adhesive coacervate. *Acta Biomater.* **10**, 1663–1670 (2014).
39. Y. Tan, S. Hoon, P. A. Guerette, W. Wei, A. Ghadban, C. Hao, A. Miserez, J. H. Waite, Infiltration of chitin by protein coacervates defines the squid beak mechanical gradient. *Nat. Chem. Biol.* **11**, 488–495 (2015).
40. D. S. Hwang, H. Zeng, A. Srivastava, D. V. Krogstad, M. Tirrell, J. N. Israelachvili, J. H. Waite, Viscosity and interfacial properties in a mussel-inspired adhesive coacervate. *Soft Matter* **6**, 3232–3236 (2010).
41. M. Rousseau, E. Lopez, A. Couté, G. Mascarel, D. C. Smith, R. Naslain, X. Bourrat, Sheet nacre growth mechanism: A Voronoi model. *J. Struct. Biol.* **149**, 149–157 (2005).
42. L. Mao Che, S. Golubic, T. Le Campion-Alsumard, C. Payri, Developmental aspects of biomineralisation in the polynesian pearl oyster *Pinctada margaritifera* var. *cumingii*. *Oceanol. Acta* **24**, S37–S49 (2001).
43. E. C. Keene, J. S. Evans, L. A. Estroff, Silk fibroin hydrogels coupled with the n16N-β-chitin complex: An in vitro organic matrix for controlling calcium carbonate mineralization. *Cryst. Growth Des.* **10**, 5169–5175 (2010).
44. N. H. Munro, K. M. McGrath, Biomimetic approach to forming chitin/aragonite composites. *Chem. Commun.* **48**, 4716–4718 (2012).
45. X. Li, Z.-H. Xu, R. Wang, In situ observation of nanograin rotation and deformation in nacre. *Nano Lett.* **6**, 2301–2304 (2006).
46. M. Rousseau, E. Lopez, P. Stempflé, M. Brendlé, L. Franke, A. Guette, R. Naslain, X. Bourrat, Multiscale structure of sheet nacre. *Biomaterials* **26**, 6254–6262 (2005).
47. E. M. Pouget, P. H. H. Bomans, J. A. C. M. Goos, P. M. Frederik, G. de With, N. A. J. M. Sommerdijk, The initial stages of template-controlled $CaCO_3$ formation revealed by Cryo-TEM. *Science* **323**, 1455–1458 (2009).
48. G. Zhang, J. Xu, From colloidal nanoparticles to a single crystal: New insights into the formation of nacre's aragonite tablets. *J. Struct. Biol.* **182**, 36–43 (2013).
49. K. P. Campbell, D. H. MacLennan, A. O. Jorgensen, Staining of the Ca^{2+}-binding proteins, calsequestrin, calmodulin, troponin C, and S-100, with the cationic carbocyanine dye "Stains-all." *J. Biol. Chem.* **258**, 11267–11273 (1983).
50. J. J. Water, M. M. Schack, A. Velazquez-Campoy, M. J. Maltesen, M. van de Weert, L. Jorgensen, Complex coacervates of hyaluronic acid and lysozyme: Effect on protein structure and physical stability. *Eur. J. Pharm. Biopharm.* **88**, 325–331 (2014).
51. E. C. Keene, J. S. Evans, L. A. Estroff, Matrix interactions in biomineralization: Aragonite nucleation by an intrinsically disordered nacre polypeptide, n16N, associated with a β-chitin substrate. *Cryst. Growth Des.* **10**, 1390–1398 (2010).

Acknowledgments: We thank K. Cho and M. S. Yoo [Pohang University of Science and Technology (POSTECH)] for assistance with the confocal Raman spectroscopy analysis and S. H. Oh and S. Lee (POSTECH) for assistance in analyzing selected area electron diffraction pattern. We also would like to thank B. Yang and H. J. Kim (POSTECH) for advice on coacervation analysis. **Funding:** The financial support for this study was provided by a Marine Biomaterials Research Center grant from the Marine Biotechnology Program of the Korea Institute of Marine Science and Technology Promotion, funded by the Ministry of Oceans and Fisheries, Korea. **Author contributions:** S.Y.B., Y.S.C., and H.J.C. designed the experiments. S.Y.B. performed the experiments. S.Y.B., B.H.J., Y.S.C., and H.J.C. analyzed the data. S.Y.B., B.H.J., Y.S.C., and H.J.C. wrote the paper. **Competing interests:** The authors declare that they have no competing interests. **Data and materials availability:** All data needed to evaluate the conclusions in the paper are present in the paper and/or the Supplementary Materials. Additional data related to this paper may be requested from the authors.

Submitted 14 March 2017
Accepted 28 June 2017
Published 2 August 2017
10.1126/sciadv.1700765

Citation: S. Y. Bahn, B. H. Jo, Y. S. Choi, H. J. Cha, Control of nacre biomineralization by Pif80 in pearl oyster. *Sci. Adv.* **3**, e1700765 (2017).